

Resistivity imaging of soil during electrokinetic transport

L.J. West^a, D.I. Stewart^{b,*}, A.M. Binley^c, B. Shaw^c

^a Department of Earth Sciences, University of Leeds, Leeds LS2 9JT, UK

^b Department of Civil Engineering, University of Leeds, Leeds LS2 9JT, UK

^c Department of Environmental Science, Lancaster University, Lancaster LA1 4YQ, UK

Abstract

Electrical resistance imaging of soil specimens during electrokinetic treatment is reported. Column experiments were carried out on Speswhite kaolinite contaminated with lead nitrate to levels both above and below its cation exchange capacity (CEC). Post test chemical analyses of the specimens and their pore fluids show that resistivity variations correlate with changes in pore fluid chemistry but do not show the extent of decontamination.

Regions of high resistivity correspond with precipitation zones within the specimens whereas regions of low resistivity correspond with regions of high pore fluid ionic strength. Where the contamination level is below the CEC, decontamination is slow as lead ions are mostly sorbed to the clay so most of the current is carried by electrolysis products and clay dissolution products. A broad resistive zone forms over the cathode half where hydroxyl and HCO_3^- ions formed in the cathode reservoir precipitate clay with dissolution products and other ions. Where the contamination level is above the CEC, lead ions are initially major charge carriers and decontamination over the bulk of the specimen is rapid. However, lead still precipitates immediately adjacent to the cathode reservoir to form a narrow resistive region. © 1999 Elsevier Science B.V. All rights reserved.

Keywords: Clays; Contaminated land; Electrokinetics; Environmental geotechnics; Pollution migration/control; Resistivity surveys

1. Introduction

Electrokinetic decontamination is a promising new technique for treating soil, where an electric current is passed through the soil inducing the migration of contaminants towards collection wells. Two primary transport processes occur: electromigration (ion movement through the pore solution towards the oppositely charged electrode) and electroosmosis (transport in the pore fluid where flow is induced by the electric field).

Electromigration occurs in all soils, whereas electroosmosis is only significant in clay soils. Advantages of electrokinetic decontamination are that it operates on the soil in situ, and can be effective in fine grained soils whose low permeability makes hydraulic flushing difficult. Many laboratory studies have been performed to characterise electrokinetic transport (e.g., Eykholt and Daniel, 1994; Hamed et al., 1991; Yeung and Mitchell, 1993), and field decontamination has been attempted (e.g. Lageman, 1993).

Monitoring of contamination levels in field studies has relied on the analysis of samples taken from discrete locations. Achieving sufficient resolution by this method for adequate process control can be time consuming and expensive. This paper

* Corresponding author. Tel.: +44-113-243-2287; fax: +44-113-233-2265.

E-mail addresses: j.west@earth.leeds.ac.uk (L.J. West), d.i.stewart@leeds.ac.uk (D.I. Stewart), a.m.binley@lancaster.ac.uk (A.M. Binley)

reports a pilot study investigating the use of electrical resistance tomography (ERT) to monitor electrokinetic soil decontamination. The objectives of this study were:

1. to determine whether ERT could be used to monitor resistivity changes induced by electrokinetic soil treatment; and
2. to determine whether these resistivity changes could be correlated with induced chemical changes within the soil (and particularly with degree of decontamination).

2. Materials

The materials used in this study were Speswhite kaolinite supplied by ECC International, analytical grade lead (II) nitrate supplied by Merck Ltd, UK, and distilled water. The adsorption isotherm for lead (II) ions at the natural pH of ca 4.5 is shown in Fig. 1 (for details of the isotherm determination see West and Stewart, 1995). Other properties of Speswhite kaolinite are listed in Table 1.

3. Experimental

The experimental programme was conducted using reconstituted kaolinite as this reproduces important properties of natural clay soils (such as low hydraulic permeability, significant electro-osmotic permeability, sorption behaviour) while

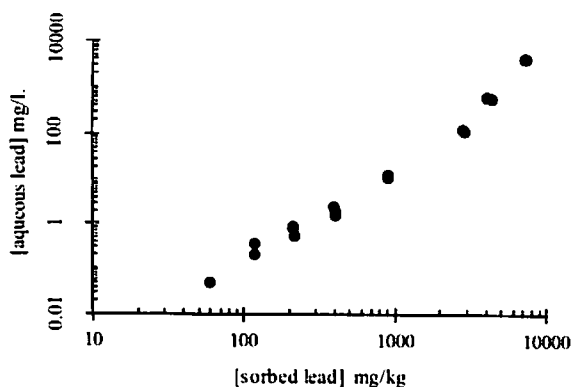


Fig. 1. Adsorption isotherm.

Table 1
Properties of Speswhite kaolinite

Characteristic	Data
Mineralogy: ^a	
Kaolinite	94%
Mica	4%
Montmorillonite	1%
Feldspar and quartz	1%
Surface area ^a (m ² g ⁻¹)	14.0
Percentage of particles (<2 μm) ^b	80%
Plastic limit ^b	38%
Liquid limit ^b	80%
Cation exchange capacity (m-equiv/100 g pH 7)	4–5

^a McGuffog, ECC International Ltd (personal communication).

^b Al-Tabbaa (1987).

keeping the system simple and repeatable. The kaolinite powder was premixed at 100% moisture content with solutions of lead (II) nitrate to ensure homogeneous specimens (which facilitates interpretation of test results). The slurry was vacuum de-aired for ca 1 h then consolidated directly into a 200 mm long, 90 mm internal diameter acrylic tube that was fitted with an extension tube. The final consolidation stress was 19.4 kN m⁻², which resulted in a moisture content of ca 67%. After consolidation, the column extension was removed and the specimens trimmed to 200 mm, and a sample was retained for analysis. Specimen details are given in Table 2.

Acrylic end-caps containing graphite power supply electrodes and porous stones were placed on each end of the tube (see Fig. 2). A gap of 3 mm between the porous stones and the power electrodes allowed fluid to be circulated between the end caps and external reservoirs by peristaltic pumps (the fluids were initially distilled water). The fluid maintained electrical contact between the specimens and the power electrodes, and prevented drying of the specimens. Also flushing of the electrode surfaces reduced power electrode polarisation, removed gas generated by electrolysis reactions and ensured thorough mixing of each fluid between internal and external reservoirs. Monitoring electrodes were installed along opposite sides of the column. The monitoring electrodes were stainless steel bolts (with locking nuts) that

Table 2
Initial specimen data

Test	Lead content after consolidation (mg kg ⁻¹)	Initial resistivity (Ω m ⁻¹)	Specimen pH	Initial electroosmotic permeability (cm ² V ⁻¹ s ⁻¹)
H4	865	13.9	4.2	2.1 × 10 ⁻⁵
H9	727	12.1	4.2	^a
H5	7650	2.7	3.3	1.2 × 10 ⁻⁵
H10	7775	2.1	3.3	1.4 × 10 ⁻⁵

^a An accurate value could not be determined due to water leakage from the reservoir.

were advanced 2mm into the specimens prior to testing, and were advanced further if measurements showed that electrical contact had deteriorated.

During testing a constant voltage of 7.5 V was applied between the power electrodes, and reservoir pH, anode reservoir mass, electric current, and the voltages at each of the seven monitoring electrodes along the front of the column were recorded at regular intervals. Periodically the anode reservoir was replenished with distilled water. Test durations were between 13 and 15 days. Periodically during tests H4 and H5 data were gathered for ERT image reconstruction (while the electrical supply to the graphite power electrodes was disconnected), using a Geopulse data acquisition unit manufactured by Campus Instruments, Birmingham, UK. A total of 298 'four-electrode'

measurements were taken using combinations of the 14 monitoring electrodes. In each measurement a 1 mA, 0.5 Hz square-wave alternating current was applied between two electrodes while measuring the potential difference between the other two electrodes. ERT data acquisition typically took 2 h.

After testing, the clay specimens were extruded and sliced into sections, and each slice was homogenised by mixing. The pH and moisture content of each slice was measured, prior to analysis for lead content using X-ray fluorescence spectroscopy. Specimens H4 and H5 were sliced into ten 20 mm thick sections, whereas specimens H9 and H10 were divided into six 33 mm thick slices. These thicker slices provided less resolution in the lead and pH profiles, but yielded sufficient clay for

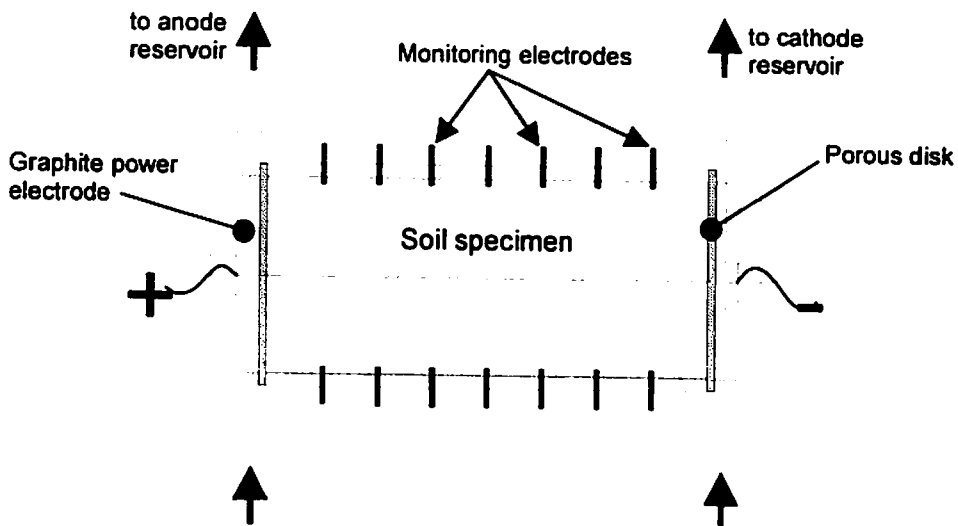


Fig. 2. Schematic diagram of the column apparatus (monitoring electrodes are shown rotated from the horizontal into the vertical plane for clarity).

a pore fluid sample to be extracted by centrifuging at 5000g for 15 min. The pore fluid pH and conductivity were measured. Pore fluid lead levels were measured by atomic adsorption spectroscopy (AAS). Other pore fluid cations and silica were measured by induction coupled plasma atomic emission spectroscopy (ICP-AES), and anion concentrations were measured by eluent suppressed ion chromatography.

3.1. Electrical resistance tomography data processing

The electrical response of a conductive media is governed by the Poisson equation, which for a source-free inhomogeneous conducting body is:

$$\nabla \rho^{-1} \nabla V = 0, \quad (1)$$

where $\rho(x, y)$ is the resistivity distribution and V is voltage. This work employed the finite element method to solve the Poisson equation for an assumed resistivity distribution, and thereby calculate a model resistance for each four-electrode combination used during ERT data acquisition. For this forward modelling step, the cylindrical specimens were represented by a two-dimensional finite element mesh of 32×14 square elements. Two layers of 14 elements at each end of the mesh represented the electrode reservoirs. These additional elements were included to minimise the influence of reservoir electrolyte resistivity variations on apparent specimen resistivity. The mesh boundaries were assumed to be non-conducting, and the variation in elemental thickness arising from a two-dimensional representation of a cylindrical specimen was incorporated into the analysis.

The inverse problem of determining an unknown resistivity distribution from measured transfer resistances containing known errors is solved by combining two constraints using the method of Lagrange multipliers. These constraints are:

1. agreement between the transfer resistances $F(m)$, calculated from an assumed resistivity distribution, m , and the measured transfer resistances, D , and
2. solution simplicity.

They can be expressed as a regularised objective

function, Φ , where

$$\Phi = [D - F(m)]^T W^T W [D - F(m)] + \alpha m^T R m. \quad (2)$$

No additional constraint was placed on resistivity. The first term on the right of Eq. (2) quantifies the differences between $F(m)$ and D by the method of weighted least squares, where W is a weight matrix which defines uncertainty in the resistance data. The second term quantifies the roughness of the solution (i.e. it is the smoothing term). The roughness matrix, R , is a geometry matrix used to identify the elements that are required to calculate the resistivity Laplace operator at a particular location, and α is the Lagrange multiplier which controls the overall contribution of the smoothing term. Here, α is determined iteratively using the approach described by deGroot-Hedlin and Constable (1990).

The inverse problem was solved using a coarser mesh than that employed for the forward problem [a common approach to ERT data reconstruction; see Binley et al. (1996)]. Each parameter block (an element used in the solution of the inverse problem) consisted of four adjacent finite elements. Minimisation of Eq. (2) with respect to parameters m is achieved numerically starting from an assumed resistivity distribution. In each iteration, the values in m are adjusted by an amount dependent on the difference between transfer resistances calculated for the assumed resistivity distribution and those that were measured. Here, iteration was stopped as soon as the data misfit was consistent with known errors in the transfer resistance measurements. For more details of ERT image reconstruction see Binley et al. (1995).

4. Results

Fig. 3 shows the electrical potentials along one row of monitoring electrodes at intervals during the tests. The initial voltage profiles in the specimens (not shown) were flat because the reservoir fluids were initially distilled water, which is relatively resistive. The reservoir fluid conductivities quickly increased (within half an hour) due to electrolysis reactions at the power electrodes and then most of the applied voltage was dropped

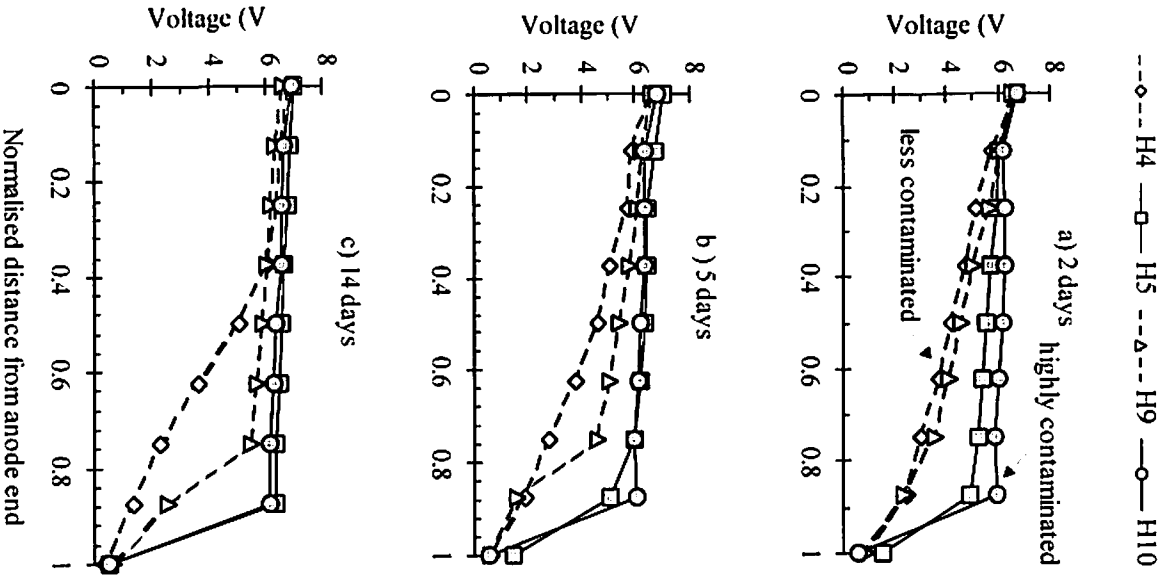


Fig. 3. Voltage profiles after 2, 5 and 14 days.

uniformly across the specimens. In the highly contaminated specimens there was localisation on the voltage profiles after 2 days, with most of the applied voltage dropped between the last monitoring electrode and the end of the specimen (in reality the voltage was probably dropped across a stiff, friable and discoloured zone ca 5 mm thick which developed immediately adjacent to the cathode). This voltage drop endured until the ends of

the tests. In the less contaminated specimens there was little variation in voltage gradient after 2 days. Later the two less contaminated specimens behaved slightly differently, with varying amounts of localisation in the cathode half of the specimens. No zone of stiff discoloured clay was observed.

Fig. 4(a and b) show the electrical current and electroosmotic flow during testing. Pore water flow was from the anode towards the cathode, and was significantly lower in those specimens contaminated with lead to levels above the cation exchange capacity. This is characteristic behaviour for Speswhite kaolinite and results from the effect of lead sorption on the zeta potential of the clay (West and Stewart, 1995). No trends or significant changes in specimen moisture content were observed after testing.

The initial resistivity of the less contaminated specimens was about five times that of the highly contaminated specimens (see Table 2). In the highly contaminated specimens, the electrical current quickly rose to ca 20 mA, but subsequently

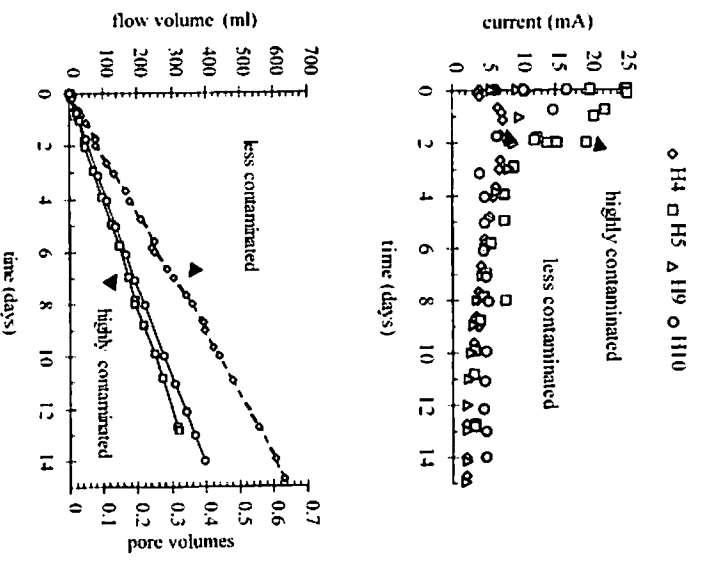


Fig. 4. (a) Electrical current and (b) electroosmotic flow (an accurate value could not be determined for specimen H9 due to leakage).

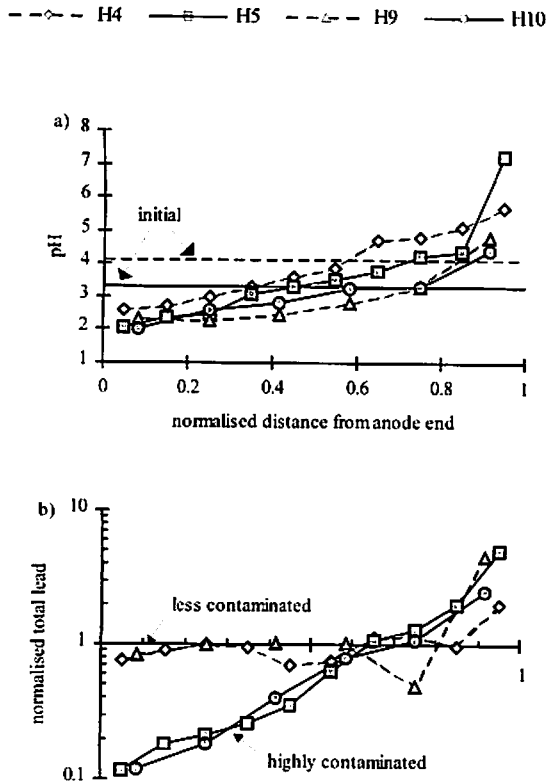


Fig. 5. (a) pH profiles and (b) normalised lead levels after testing.

fell sharply to ca 7 mA after 4 days. It had fallen to ca 4 mA by 14 days. In the less contaminated specimens, the electrical current quickly rose to ca 10 mA and then fell gradually through the remaining test period to 2 mA.

Fig. 5(a and b) shows the pH profiles (measured by inserting the pH electrode directly into the clay) and the normalised total lead levels after testing. As a result of producing H⁺ at the anode and OH⁻ at the cathode by electrolytic decomposition

of water, the pH of all specimens decreased towards pH 2 in their anode halves and increased towards pH 8 in the soil close to the cathode (the pH was initially ca 4). Significant lead removal occurred over two thirds of the highly contaminated specimens (greatest near the anode), whereas there was comparatively little lead depletion in the less contaminated specimens. This was because most of the lead was sorbed to the clay in the less contaminated specimens. Lead accumulated adjacent to the cathode in all specimens, although the absolute lead levels in this region were much higher in the highly contaminated specimens.

Table 3 gives the major ions in the extracted pore fluid from specimens of the consolidated clay before use in tests H9 and H10 (charge balance errors were <4%, so it is probable that all the major charged species were detected). The initial pore fluid concentrations of alkali and alkaline earth metal ions were higher in specimen H10 than in specimen H9 as a result of extensive displacement from exchange sites by lead. Table 3 indicates that the major pore fluid ions at the start of test H9 were sodium, nitrate and to a lesser extent sulphate ions (i.e. most of the lead was sorbed to the clay). In the highly contaminated specimen H10, the major pore fluid ions were initially lead, nitrate and to a slightly lesser extent sodium ions (i.e. the lead level exceeded the CEC, so substantial quantities remained in solution).

Figure 6 shows the concentrations of major species in the pore fluid extracted from the specimens and in the anode and cathode reservoir fluids at the end of tests H9 and H10 (note that the fluid volume in each reservoir was similar to the pore volume of the entire specimens so the data for reservoirs represent relatively large quantities of ions). Hydrogen and hydroxyl concentrations shown in Fig. 6 were calculated from the pore fluid

Table 3
Composition of the extracted pore fluid (mmol l⁻¹)

Specimen	H ⁺ ^a	Na	K	Ca	Mg	Fe	Al	SiO ₂	Pb	NO ₃	SO ₄	Cl
H9	0.02	11.24	0.9	0.64	0.51	0.01	0.06	0.87	0.28	8.9	2.8	0.7
H10	0.35	16.7	2.67	3.73	4.32	0.04	1.69	1.6	27.4	85	2.8 ^b	0.7 ^b

^a Calculated from the pH by assuming unit hydrogen ion activity.

^b Assumed values, not measurable by ion chromatography due to the large amount of nitrate present.

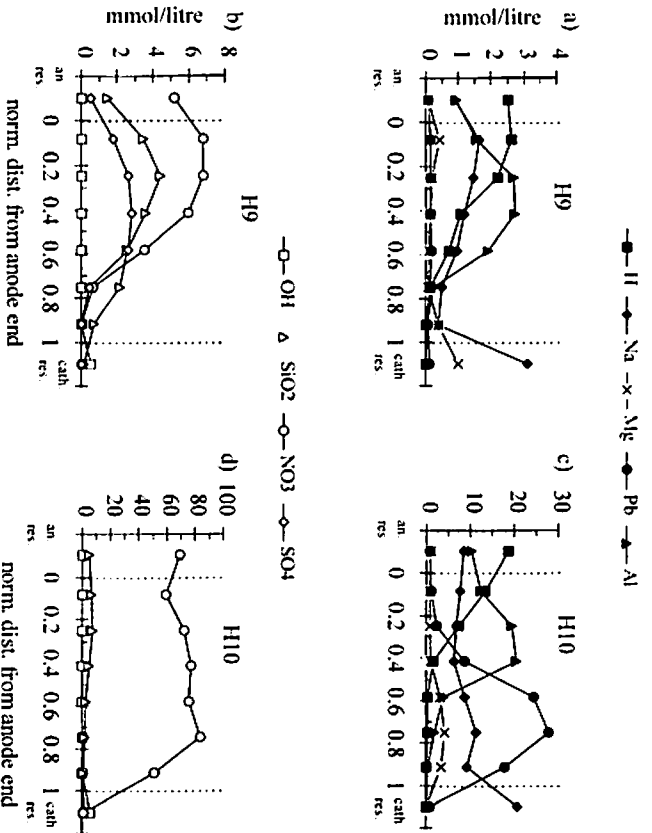


Fig. 6. Pore fluid species after testing.

pH by assuming unit activity for hydrogen ions. After 2 weeks of voltage application, sodium and other alkali and alkaline-earth cation concentrations in the pore fluid had reduced over most of specimen H9 [see Fig. 6(a)]. These cations accumulated mainly in the cathode reservoir (surprisingly some sodium also entered the anode reservoir probably as the result of diffusion). The levels of major anions (nitrate and sulphate) reduced near the cathode and increased in the anode reservoir, but remained essentially unchanged in the anode half of the specimen [see Fig. 6(b)]. Lead was not a major ion in the pore fluid anywhere in specimen H9.

During test H10 sodium and other alkali cations were depleted throughout the specimen, accumulating mainly in the catholyte [see Fig. 6(c)]. Nitrate was depleted near the cathode, remained essentially unchanged in the bulk of the specimen, and accumulated in the anode reservoir [see Fig. 6(d)]. Pore fluid lead levels were highest (near their initial value) between normalised distances of 0.6–0.8 from the anode, but were lower elsewhere [see Fig. 6(c)]. Both pH conditions and charge balance considerations indicate that pore

fluid lead was Pb^{2+} . The lead distribution indicates that Pb^{2+} migrated towards the cathode where it precipitated.

Aqueous aluminium and silica levels rose in both specimens, except near the cathode (see Fig. 6). This aluminium and silica probably results from breakdown of the clay lattice in the acidic conditions near the anode [according to Grim (1968), the octahedral layers of kaolinite can decompose in acid conditions]. This deduction has been confirmed by batch acid extractions on Speswhite kaolinite using dilute HNO_3 . These showed elevated levels of silica and aluminium when the pH was about 2. Both pH and charge balance considerations indicated that dissolved aluminium is present as Al^{3+} and silica is neutral [these are the thermodynamically favoured forms of aluminium and silica at the prevalent pH; Portaux (1966)]. Most of these dissolution products were transported towards the cathode by electromigration and electroosmosis, but some entered the anolyte by diffusion. Electrokinetic transport back into the specimen was inhibited because the anolyte was circulated to an external reservoir outside the electric field.

The measured ionic compositions of the catholyte and pore fluid from the cathode slice of specimen H9 indicate deficits in negative charge of 5 and 1.5 m-equiv l^{-1} , respectively. These deficits probably indicate that carbonate species such as HCO_3^- were present. Such anions were probably produced by the reaction of atmospheric carbon dioxide with hydroxyl ions as the cathode reservoir was open to the atmosphere. Similar considerations suggest that 21 m-equiv l^{-1} of carbonate species were present in the catholyte of test H10. Further evidence that carbonate ions were present in the catholyte is provided by analyses of precipitates from the cathode region of specimen H10, which indicate the presence of lead carbonates (S.R. Johnston, personal communication).

5. ERT images

Figs. 7 and 8 show ERT images along the horizontal axial plane of the specimens H4 and H5, respectively, at selected times during the tests (the initial resistivity of both specimens was uniform). Logarithmic scales have been used for resistivity, and note that different scales are used

on the two figures. ERT does not provide unique solutions to the inverse problem and local variations [such as the 'X' structure in the resistive zone in Fig. 7(b)] are artefacts of the electrode configuration and inversion technique employed. Also, resistive features narrower than the resolution of the technique will be smeared out (for example, ERT gave a catholyte resistivity in excess of the measured value for test H5, due to the proximity of the highly resistive precipitation zone). However, the broad patterns of resistivity discernible in Figs. 7 and 8 result from changes in resistivity.

Fig. 7 suggests that the resistivity of the less contaminated specimen H4 had changed little after 2 days, but a heterogeneous resistivity distribution had developed after 4 days of current application. By 13 days of current application the image shows two distinct zones of resistivity. Near the anode the specimen resistivity was essentially unchanged (the ERT images indicate a conductive anomaly had developed adjacent to the anode after 4 days, but this had diminished in size by the end of the test). ERT indicates that the resistivities in the cathode half of the specimen H4 increased substantially, with final values well in excess of 100 Ωm .

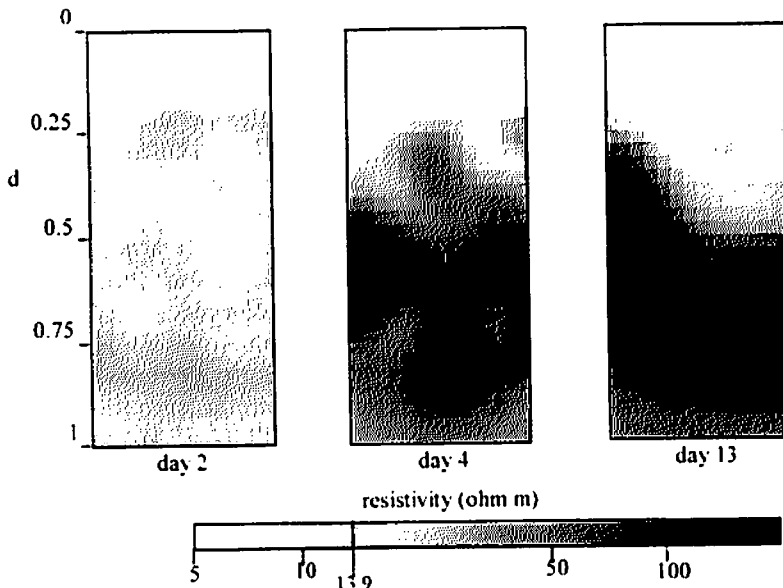


Fig. 7. Resistivity distribution for specimen H4 (initial resistivity $13.9 \Omega m^{-1}$).

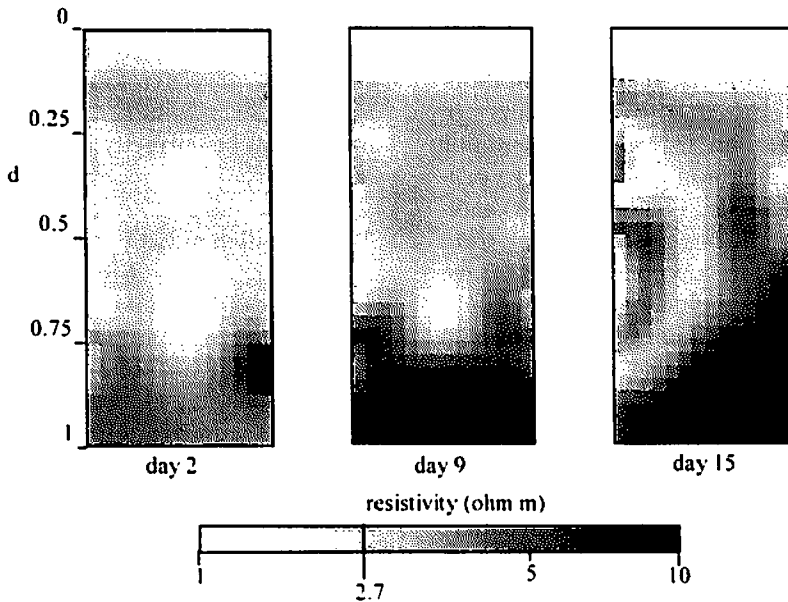


Fig. 8. Resistivity distribution for specimen H5 (initial resistivity $2.7 \Omega \text{ m}^{-1}$).

The ERT images of the highly contaminated specimen H5 show that a resistive zone developed near the cathode, detectable after 2 days [Fig. 8(a)] and fully developed after 9 days of testing [Fig. 8(b)]. This zone was thinner and less resistive than the resistive region in the ERT images of specimen H4. Fig. 8 indicates that the resistivity of the remainder of the specimen H5 did not change much during the test.

6. Discussion

The fractional contribution of each ion to the extracted pore fluid conductivity (its transport number) was calculated by assuming that the deviation from ideal behaviour within the pore fluid from each slice was the same for all ions. Note that such transport numbers are only a guide to the transport numbers within the specimens, where other effects such as diffusion and electroosmotic flow will influence ionic transport (Alshawabkeh and Acar, 1996). Major contributors to pore fluid conductivity (defined here as ions with transport numbers >0.1) at the start of test H9 were sodium, nitrate and sulphate ions, whereas the major con-

tributors at the start of test H10 were lead and nitrate ions. Fig. 9 shows the distribution of major contributors in both specimens after 2 weeks of voltage application. Within the sub-regions indicated in Fig. 9 the major contributors were the

Anode Res.	Soil Specimen					Cath. Res.
H^+ Al^{3+}	H^+ Al^{3+}	Al^{3+} H^+	H^+ Al^{3+}	Mg^{2+} Ca^{2+} Na^+	Na^+ K^+	
NO_3^-	NO_3^- SO_4^{2-}	SO_4^{2-} NO_3^-	SO_4^{2-} HCO_3^- NO_3^-	HCO_3^-	HCO_3^- OH^-	

(a) Specimen H9

Thin discoloured region
↓

H^+ Al^{3+}	H^+ Al^{3+}	Al^{3+} H^+	Al^{3+} Pb^{2+}	Pb^{2+}	?	Na^+
NO_3^-			NO_3^-		?	OH^- HCO_3^-

(b) Specimen H10

Fig. 9. Distribution of major contributors to extracted pore fluid conductivity after 2 weeks of voltage application.

same, although ionic concentrations varied substantially across sub-regions.

All the tests were dominated by precipitation/neutralisation reactions due to the entry of hydroxyl and HCO_3^- anions from the cathode reservoir, and the dissolution of kaolinite to produce Al^{3+} near the anode. Fig. 6(b and d) indicates that few hydroxyl ions progressed far from the cathode reservoir in any of the specimens. However, the less contaminated specimens exhibited a broad resistive precipitation zone [seen in the ERT image of specimen H4 after 4 days of current application, Fig. 7(b)]. This zone probably results from precipitation of Al^{3+} , or neutralisation of H^+ , with HCO_3^- (rather than OH^- ions). In the highly contaminated specimens, the much higher availability of lead restricted carbonate precipitation to a narrow zone near the cathode, which started to show up after 2 days of current application as a narrow resistive zone on the ERT image (Fig. 8).

In the highly contaminated specimens aqueous lead remained a major charge carrier in cathode half after 15 days, which indicates that decontamination was ongoing. The interface between the regions where aluminium and lead were major charge carriers cannot be seen on the ERT images of specimen H5, because these regions had similar resistivities. Thus, ERT detected precipitation/neutralisation events during electrokinetic treatment, but could not distinguish contaminant transport from that of other ionic species.

Reactions such as alkali production and atmospheric carbonation, and subsequent precipitation of carbonates and hydroxides are likely to occur in most soils unless the catholyte pH is controlled during electrokinetic treatment. However, the extent of acidification by anode electrolysis will depend on the soil buffer capacity. For kaolinite, buffering involves the dissolution of the octahedral layers of the clay lattice. Other clay minerals are subject to similar reactions. However, natural soils containing carbonate grains and/or iron and manganese oxide coatings will be buffered at a higher pH by the dissolution of these phases (delaying or preventing clay dissolution). Although the final pH of the soil will be a function of the buffering reaction, buffering invariably involves the release

of other ions from the soil. Using ERT to monitor electrokinesis therefore requires a phenomenological model of electrokinetic treatment, including reactions such as mineral dissolution, so that the images can be correctly interpreted.

7. Application of ERT at field scale

The use of ERT imaging to characterise geological structure is commonplace [e.g. Andrews et al. (1995), used a surface array to perform field scale electrical imaging at sites on the unsaturated zone of a chalk aquifer]. More recently the technique has been used to monitor conductive tracer transport [e.g. Slater et al. (1997) monitored preferential flow through unsaturated Chalk using electrodes spaced at 1.5 m intervals down two boreholes]. As resistivity changes arising from electrokinetic transport are similar to those arising from hydraulic transport, ERT is expected to be suitable for monitoring electrokinetic decontamination.

When using either surface or borehole electrode arrays, image resolution is fundamentally limited by the monitoring electrode spacing. Maximum resolution is achieved where the domain of interest lies directly between electrodes. Downhole electrodes are therefore required to give good resolution at depth. In any application, the current level is selected to produce potential differences between the measurement electrodes that are large compared with the natural potential variations in the ground, and is usually in the range 2–20 mA.

8. Conclusions

- When the anode reservoir is not buffered, hydrogen ions produced by electrolysis will attack the kaolinite and produce Al^{3+} , which becomes the a major charge carrier. When the cathode reservoir is not buffered, precipitation of hydroxides and carbonates will increase soil resistivity locally.
- ERT can be used to monitor resistivity changes induced in laboratory specimens by electrokinetic soil treatment, and these resistivity changes

correlate with chemical changes within the soil (although not directly with the extent of decontamination).

- ERT may provide a suitable tool for monitoring electrokinetic remediation in the field. It can be used to identify precipitation events but a phenomenological model of electrokinesis is required to correctly interpret the chemical significance of these events.

Acknowledgements

The authors would like to acknowledge the support of the EPSRC through Grant Nos GR/J09932 and GR/K57770. The authors would also like to thank Dr S.R. Johnston and Dr D. Banks for conducting the chemical analyses of the pore solutions.

References

- Alshawabkeh, A.N., Acar, Y.B., 1996. Electrokinetic remediation. II: Theoretical model. *ASCE J. Geotechnical Eng.* 122 (3), 186–196.
- Al-Tabbaa, A., 1987. Permeability and stress strain response of Speswhite kaolinite. Ph.D. thesis, University of Cambridge, Cambridge, UK.
- Andrews, R.J., Barker, R., Loke, M.H., 1995. The application of electrical tomography in the study of the unsaturated zone in chalk at three sites in Cambridgeshire, United Kingdom. *Hydrogeol. J.* 3, 17–31.
- Binley, A.M., Ramirez, A., Daily, W., 1995. Regularised image reconstruction of noisy electrical resistance tomography data. In: Beck, M.S., Hoyle, B.S., Morris, M.A., Waterfall, R.C., Williams, R.A. (Eds.), *Process Tomography '95: Implementation for Industrial Processes*. UMIST, Manchester, pp. 401–410.
- Binley, A.M., Shaw, B., Henry-Poulter, S., 1996. Flow pathways in porous media: electrical resistance tomography and dye staining image verification. *Measurement Sci. Technol.* 7 (3), 384–390.
- deGroot-Hedlin, C., Constable, S., 1990. Occam's inversion to generate smooth, two-dimensional models from magnetotelluric data. *Geophysics* 55 (12), 1613–1624.
- Eykholt, G.R., Daniel, D.E., 1994. Impact of system chemistry on electroosmosis of contaminated soils. *ASCE J. Geotechnical Eng.* 120 (5), 797–815.
- Grim, R.E., 1968. *Clay Mineralogy*. 2nd ed., McGraw-Hill, New York.
- Hamed, J., Acar, Y.B., Gale, J.G., 1991. Pb(II) removal from kaolinite by electro-kinetics. *ASCE J. Geotechnical Eng.* 117 (2), 241–271.
- Lageman 1993. *Electroreclamation: applications in the Netherlands*. *Environ. Sci. Technol.* 27, 2648–2650.
- Porbaix, M., 1966. *Atlas of Electrochemical Equilibria in Aqueous Solutions*. Pergamon Press, London.
- Slater, L., Zaidman, M.D., Binley, A.M., West, L.J., 1997. Electrical imaging of saline tracer migration for the investigation of unsaturated zone transport mechanisms. *Hydrol. Earth System Sci.* 1, 291–302.
- West, L.J., Stewart, D.I., 1995. Electrokinetic decontamination: the effect of zeta potential. *Geoenvironment 2000*. *Am. Soc. Civil Eng. Special Publication* 46, 1535–1549.
- Yeung, A.T., Mitchell, J.K., 1993. Coupled fluid, electrical and chemical flows in soil. *Geotechnique* 43 (1), 121–134.